THE JOURNAL OF PHYSICAL CHEMISTRY C

Article

Cite This: J. Phys. Chem. C 2018, 122, 28151−28157

pubs.acs.org/JPCC

Surface Chemistry and Long-Term Stability of Amorphous Zn−Sn−O Thin Films

Stephanie L. Moffitt,[†] D. Bruce Buchholz,[†] Robert P. H. Chang,[†] Thomas O. Mason,[†] Tobin J. Marks,[‡] Michael J. Bedzyk,[†] and Qing Ma*[,§]

[†]Materials Science and Engineering Department, Northwestern University, Evanston, Illinois 60208, United States

[‡]Chemistry Department, Northwestern University, Evanston, Illinois 60208, United States

[§]DND-CAT, Northwestern Synchrotron Research Center at the Advanced Photon Source, Argonne, Illinois 60439, United States

Supporting Information

ABSTRACT: Amorphous (*a*-) oxides form an important category of transparent conducting/semiconducting thin films used as electrodes and channel layers in thin film transistors. The compositional flexibility of amorphous states, through doping, makes it possible to fine-tune the electrical properties of films from conducting to semiconducting. However, surface chemistry and stability of these films are rarely addressed. Surface studies of amorphous materials, in general, are scarce due to disorder. Here, long-term surface stability of *a*−Zn−Sn−O films was investigated using grazing incidence X-ray absorption spectroscopy techniques. We present a detailed description of film surface structures and their evolution over time. It was found that the surface structure is, locally, a close analogue of the crystalline counterpart and that surface chemistry is governed by vacancies, strain, composition, and film density. It is shown that the long-term stability of a film is questionable when the film has a high Zn content and a low density.

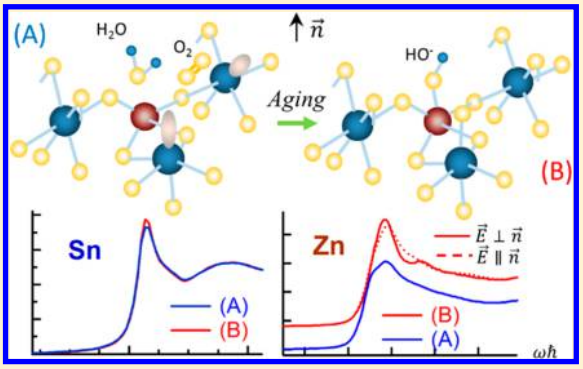

1. INTRODUCTION

Knowledge of the structure−property relationships for amorphous (*a*-) transparent conducting and semiconducting oxide (*a*-TCO and *a*-TSO) thin films is growing[1−5] due to interest in their deployment in flat panel displays. Amorphous oxides have clear advantages over their crystalline counterparts. For instance, they are considered to have better mechanical stability under stress[6,7] and have smoother surfaces.[8] They can be deposited at low temperatures on flexible substrates and thus are good candidates for flexible transistors[8,9] where sharp interfaces are desired. The compositional flexibility of the amorphous state enables fine-tuning of film electrical properties from conducting to semiconducting.[10,11]

While In_2O_3-based *a*-TCO and *a*-TSO are the most prevalent,[1] *a*-SnO_2-based films, such as Zn doped SnO_2 films (ZTO), have been explored for economic benefit because Sn is a much more abundant element than In.[12] Zhu et al. studied the local structures of ZTO films with up to 30% Zn, based on which an understanding of the electrical properties and crystallization temperature was developed.[3] The local structures of ZTO films retain rutile (SnO_2) characteristics. In rutile SnO_2 (Space group: $p42/mnm$), Sn has 6 O nearest neighbors at an average distance of 2.06 Å. In amorphous Zn-doped SnO_2 (*a*-ZTO) films, Sn is under-coordinated by 0.3 ± 0.2 O atoms with the bond distance R_{Sn-O} = 2.06 Å, while Zn is 4-fold coordinated in a distorted octahedral site with R_{Zn-O} = 1.98 Å. The oxygen vacancies around Sn are likely the source of charge carriers in ZTO. The low-coordinate Zn−O polyhedra play little role in charge balance. However, they play an important role in the thermal stability of these films. As the Zn content is increased up to 30 atom %, the crystallization temperature rises from 420 to 600 °C.

However, a question that begs an answer is what is the long-term stability of ZTO films, in particular the ones in which heavy substitution occurs, such as 30 atom % Zn substitution of Sn[3] that is believed to be far beyond the solubility limit.[13] Address of this question should be of fundamental and technological importance. Here, we studied the long-term stability of the surface structures of the *a*-ZTO films to shed light on ZTO film stability itself. Studies of amorphous surfaces in atomistic details are challenging due to their disordered nature, which inhibits the use of many common structural characterization tools and methods. Grazing incidence X-ray absorption spectroscopy (GIXAS) presents a unique way to unravel the element-specific structure of a surface. When the X-ray incidence angle (θ) is smaller than the critical angle (θ_c) of a surface, the probing depth (Λ) is only a couple of nanometers.[14] Detailed structure around Zn and Sn on the

Received: September 26, 2018
Revised: November 25, 2018
Published: November 26, 2018

DOI: 10.1021/acs.jpcc.8b09412
J. Phys. Chem. C 2018, 122, 28151−28157

surface is presented as a function of aging in air. Changes in surface structure and chemistry occur to various extents, depending on the film composition, density, and deposition conditions. These changes are prominent for low density and high Zn content films.

2. EXPERIMENTAL METHODS

Sample Preparation. *a*-ZTO films were deposited on 1 × 2 cm^2 fused silica substrates at room temperature by a pulsed laser deposition (PLD) system employing a 248 nm KrF excimer laser. The laser beam was focused to a 1 × 2 mm^2 spot size on the targets, which were rotated to prevent localized heating. A dual-target (ZnO and SnO_2) deposition method was used. Film compositions were controlled by the pulses delivered to the targets and were verified by X-ray fluorescence measurements. The *a*-ZTO films with 10 and 30% Zn doping were grown under oxygen partial pressures (pO_2) = 10, 14, and 18 mTorr, respectively, named ZTO10 and ZTO30. One *a*-SnO_2 film was also grown with pO_2 = 22 mTorr. The films prepared at pO_2 = 10 mTorr are not as transparent, having a brown hue due to presence of Sn^{2+} ions. The film thicknesses were measured by optical ellipsometry to be ∼530 nm. The electrical properties of the films were measured by Hall effect in van der Pauw configuration using an Ecopia HMS-3000 Hall system. All the films are X-ray diffraction amorphous and aged in air over a two year period in a climate-controlled laboratory. Typical humidity is between 25 and 30%, and temperature is around 20.0 °C.

X-ray Characterization. Experiments were carried out at the 5-BMD beamline of the DND-CAT at the Advanced Photon Source (Argonne, IL). A double Si (111) crystal monochromator was used for energy selection with energy resolution of $\Delta E/E = 1.4 \times 10^{-4}$. The incident X-ray intensity was measured by an ion chamber (FMD Oxford, Ltd.) and detuned to 60% of its maximum for harmonic rejection. Because the synchrotron X-ray beam is linearly polarized and the polarization vector $\vec{E}$ is in the horizontal plane, the measurements with the surface parallel (∥) and perpendicular (⊥) to $\vec{E}$ were carried out to probe structural anisotropy. A 2-circle (θ and χ) Huber stage or a 1-circle rotation stage was used in the $\vec{E}$ dependence measurements. In each case, the X-ray reflectivity (XRR) and fluorescence (XRF) off the surface were measured simultaneously using the ion chamber located downstream of the sample and using two 4-element Si-drift solid state detectors (Hitachi, Corp) located 90° to the X-ray beam, respectively. An experimental setup is shown in Figure S1 in the Supporting Material. The GIXAS spectra of both Zn K and Sn K edges are measured in fluorescence mode under the $\theta \leq \frac{2}{3}\theta_c$ condition, in which complication of the resonance effect vanishes[15] in addition to the self-absorption effect. The beam size was set to 0.05 × 8 mm^2 ($V \times H$) for Zn K edge and to 0.02 × 8 mm^2 for Sn K edge.

Reference Materials. For quantitative analyses of the GIXAS data, powder SnO_2 and ZnO (Sigma-Aldrich, 99.99%) were used to obtain the amplitude scaling factors S_0^2 (Section 2 in the Supporting Materials), 0.9 for ZnO and 1.02 for SnO_2. Powder $Zn(OH)_2$ was lab prepared using the Na(OH) and $Zn(NO_3)_2$ solutions. Powder samples were uniformly spread onto Scotch tapes (3M, Corp) which were then folded various times to achieve absorption steps ranging from 0.6 to 1. Sample uniformity was checked by using a 0.5 × 0.5 mm^2 X-ray beam scanning over the sample. The variation in the transmitted X-ray intensities is within 2% (SD). X-ray absorption measurements of these samples were carried out in transmission mode using the ion chambers. Zn and Sn metal foils (EXAFS Materials) were used for energy calibrations. For Zn K edge, gas mixtures are N_2/He = 143/506 Torr for the first ion chamber and 290/970 Torr for the second ion chamber. For Sn K edge, it is Ar/N2 = 16/540 and 36/1360, respectively.

3. RESULTS

Preliminary GIXAS results on the surface of the as-deposited ZTO30 film were described in the 16th XAFS conference.[16] It was shown that unlike in the bulk of the film where Zn is severely under coordinated (N < 4), Zn is fully coordinated (N = 4) on the surface. Sn has N ∼ 5.6 on the surface vs ∼5.9 in the film. The Sn−O and Zn−O bond distances for both Sn−O and Zn−O on the surface do not deviate from those found in the bulk of the film. Figure 1A shows the θ-dependent XRR and XRF, which was used to determine the measuring condition for the GIXAS. Figure 1B shows the X-ray absorption near edge structure (XANES) of the as-deposited ZTO30 film prepared at pO_2 = 18 mTorr (ZTO30−18 mT), which is representative of all the films, regardless of the composition and deposition pO_2. The Zn K_α and Sn Kα emission intensities mimic closely to Λ versus θ (Figure S2). Surface XANES were measured at θ = 0.18° and 0.06° for Zn K and Sn K edges, respectively, while the XANES of film bulk was measured with the film held vertically with θ = 54°. The differences seen are due to the differences in the coordination numbers (N) mentioned above. The height of the sharp peak in the XANES, "whiteline", is proportional to N. The elevated absorption before the rise of the Sn K edge for the surface over the film bulk is likely due to surface vacancies (as discussed further below).

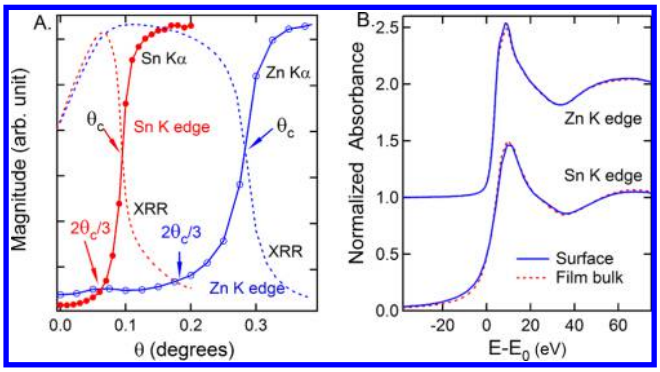

Figure 1. (A) XRR and XRF versus θ measured at 50 eV above the Zn (9658.6 eV) and Sn (29200 eV) K edges, for which θ_c is determined to be ∼0.29° and ∼0.10°, respectively. For homogeneous films, the θ dependences of XRR and XRF are complementary. (B) Comparison of surface (blue solid lines) to bulk film (red dashed lines) XANES measured at Zn (top) and Sn (bottom) K edges.

Film Densities. The XRR allows for an estimation of the film density ρ via the optical constant δ, which may be determined via simulation using the Fresnel equation[17] or using the relationship $\delta = \theta_c^2/2$, for which θ_c can be obtained from the first derivative of the XRR curves. Figure 2A shows as an example the XRR data measured on the ZTO30−18 mT film (solid line) and the Fresnel simulation (dashes). In the

DOI: 10.1021/acs.jpcc.8b09412
J. Phys. Chem. C 2018, 122, 28151−28157

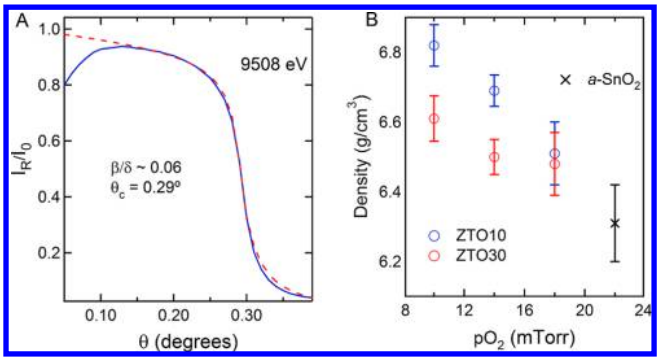

Figure 2. (A) XRR (solid line) of the *a*-ZTO30−18 mTorr film and the calculation (dash line) using the Fresnel equation: $\frac{I_R}{I_0} = \frac{[h-\gamma\sqrt{2(h-1)}]}{h+\gamma\sqrt{2(h-1)}}$,[17] where $h = \gamma^2 + \sqrt{(\gamma^2-1)^2 + \left(\frac{\beta}{\delta}\right)^2}$ and $\gamma = \frac{\theta}{\theta_c}$. (B) Film density versus pO_2. ZTO films are shown as blue and red circles. SnO_2 is shown as black ×.

simulation, θ_c and β/δ were adjusted until a reasonable fit to the data was achieved. The optical constants β and δ are on the order of ~8×10^{-7} and ~1.32×10^{-5}, respectively. The film densities derived from these θ_c values are shown in Figure 2B and show a clear pO_2 dependence, decreasing with increasing pO_2. The error bars (Figure 2B) include the differences in θ_c determined by the Fresnel calculations and the first derivatives method.

To monitor the evolution of the local structures around Zn and Sn on film surfaces over time, the GIXAS data were collected with a time increment of about one year over a two year period. The data collected on the surfaces of as-deposited, one-year aged, and two-year aged films are indicated using the subscript of *f*, a_1, and a_2, respectively. Over this time, there is a buildup of a low density carbonaceous layer on the surface, which is also appreciable (Figure S3).

Aging Effect on Surface Zn Sites. Figure 3 presents the surface Zn K edge XANES spectra of the *a*-ZTO30−18 mT film over time (A) and of the other films after the second year of aging (B). The surface structure, and likely the chemistry as well, around Zn underwent a drastic change on the *a*-ZTO30−18 mT surface. The change on the *a*-ZTO10−18 mT surface is characteristically similar, but to a lesser extent (Figure 3B). It is very small, if any, for the other films. Therefore, the films prepared with high pO_2 and higher Zn concentration are more vulnerable to surface degradation. These changes slow over time because μ_{a_2} is only slightly different from μ_{a_1}.

The Zn K edge XANES of the aged *a*-ZTO30−18 mT film bears resemblance to that of $Zn(OH)_2$ (Figure 3A). Careful examination shows that with the changes in the spectral characteristics, the Zn K absorption edge shifts by ~0.3 eV over time and is better aligned to that of $Zn(OH)_2$ (Figure S4). Therefore, protonation of the surface by hydration has likely occurred on the surfaces of the *a*-ZTO films prepared with pO_2 = 18 mTorr. Note that after aging, the initial part of the edge rise in fact aligns with that of the film (Figure S4). This may occur if hydration predominately occurs within a depth smaller than the X-ray probing depth (<3 nm, Figure S2) or if some Zn sites are not hydrated.

The X-ray polarization dependence measurements show that the surface structure displays a strong anisotropy around Zn after aging. The feature "a" (Figure 3A) is due to an increase of the σ^* character in the bonding orbital by H addition. It is thus

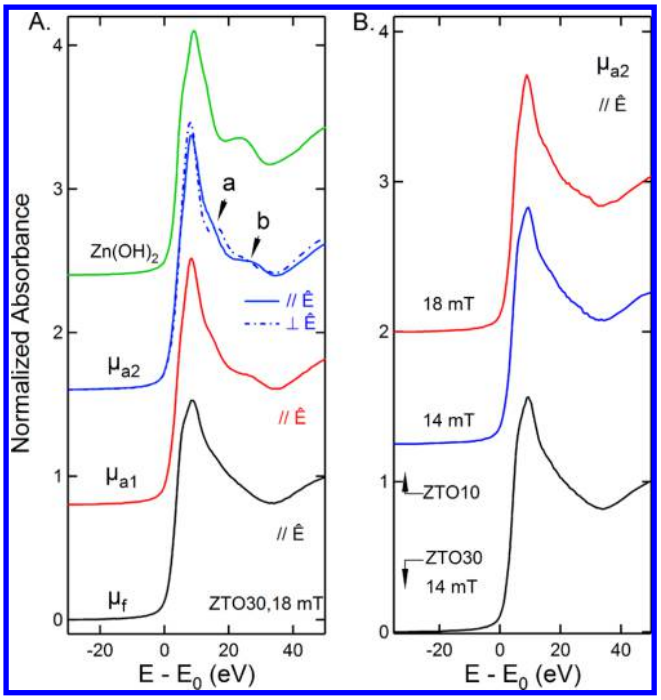

Figure 3. Zn K edge XANES as a function of time. (A) Surface XANES measured on *a*-ZTO30−18 mT with the surface ⊥ $\vec{E}$ or ∥ $\vec{E}$. Fresh (μ_f) (black line), after 1 year (μ_{a_1}) (red line), and after 2 years(μ_{a_2}) (blue lines). See the main text for description of features *a* and *b*. Also present is the XANES of $Zn(OH)_2$ for comparison (green line). (B) Surface XANES measured on the aged *a*-ZTO films with surface ∥ $\vec{E}$. Two year-old: ZTO10 deposited under 18-mTorr O_2 (red line) and under 14-mTorr O_2 (blue line), respectively, and ZTO30 deposited under 14-mTorr O_2 (black line).

assigned to a Zn−O−H interaction. It is strong when measured with the surface ⊥ $\hat{E}$, but weak with the surface ∥ $\hat{E}$; its intensity is a $\cos^2\phi$ projection of hydroxyl interaction along $\hat{E}$ (ϕ is the angle between $\hat{E}$ and the Zn−O−H bond). This indicates that the O−H bonds orient toward $\hat{n}$. The strong O−H interaction along the $\hat{n}$ direction is also corroborated by a shift of ~0.7 eV of the absorption edge measured in the ⊥ $\hat{E}$ geometry, as shown in Figure 4A. To further support this assignment, modeling by the full multiscattering (FMS) calculations using the FDMNES code[18] was carried out and is shown in Figure 4B. Upon hydrogen addition, the shoulder becomes more intense, and the absorption edge undergoes a chemical shift (~0.6 eV), which agrees with our experimental results.

The "b" feature (Figure 3A) is due to the interaction at longer distances. It is weak for the data measured with the surface ⊥ $\hat{E}$. Figures 4C and D show, respectively, the extended X-ray absorption fine structures (EXAFS) and their Fourier transforms (FT) measured on the aged *a*-ZTO30−18 mT surface, compared to $Zn(OH)_2$. It is seen that the ⊥ $\hat{E}$ EXAFS ($k > 2.4$ Å^{-1}) shows a single sinuous oscillation, while the ∥ $\hat{E}$ EXAFS is more complex. As a consequence, only the first coordination shell is seen in the FT of the ⊥ $\hat{E}$ EXAFS, while the strong second shell interaction is seen in the FT of the ∥ $\hat{E}$ EXAFS. In comparison (Figure 4D), the surface structure around Zn is very different from that of $Zn(OH)_2$, which removes the likelihood of bulk-like $Zn(OH)_2$ aggregation on

DOI: 10.1021/acs.jpcc.8b09412
J. Phys. Chem. C 2018, 122, 28151−28157

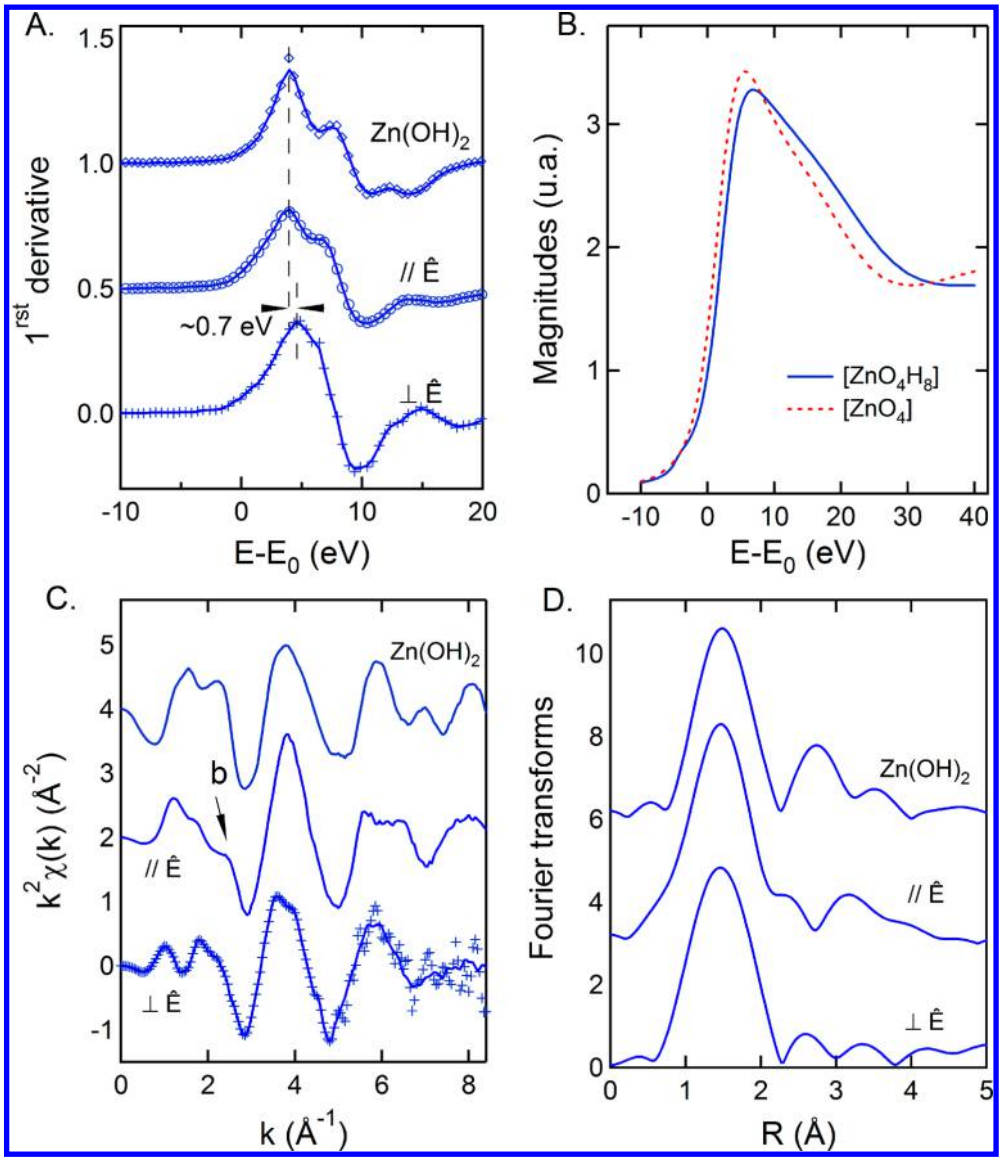

Figure 4. Surface structure measured in two geometries on the aged *a*-ZTO30−18 mT film, compared to $Zn(OH)_2$. (A) First derivatives of μ presented in Figure 2A. (B) FMS calculations: effect of hydration on XANES region. (C) EXAFS. (D) FTs of EXAFS with k = 2.3−7.6 Å^{-1}.

the surface. This interpretation can also be readily applied to the *a*-ZTO10−18 mT film, for which the changes are weaker. Therefore, the surface Zn sites of the *a*-ZTO films prepared with higher pO_2 are susceptible to hydration and undergo a structural ordering, as evidenced by the anisotropy and by the strong second shell interaction along the surface direction.

Structure of Surface Zn Sites. Surface Zn appears to be coordinated by ∼4 O for all as-deposited films. Upon aging, structural changes are appreciable in the films prepared at pO_2 = 18 mTorr. Table 1 compares the local structures for the fresh (*f*) and aged (*a*) *a*-ZTO30−18 mT film. The Zn−O bond distance is somewhat larger after aging, likely as a consequence of the increase in the coordination number. In addition, some oxygen is found around Zn at 2.79 Å, and the Zn−Sn interaction is pushed apart to 3.75 Å, which is equivalent to the fourth shell around Sn in *c*-SnO_2 and where 10 Sn cations are present. Moreover, some Zn−Zn interaction is found at 3.82 Å. Given the high Zn content, this may not be surprising. There are still some discrepancies in the fitting (Figure S5), which could belong to the Zn−Sn interaction remaining at ∼3.20 Å. Note that it is unclear if part of the increase in the coordination number around Zn is due to dissociative O_2 adsorption.

Table 1. Surface Structures around Zn of As-Deposited (*f*) and Aged Films (*a*)[a]

	N		*R* (Å)		$\sigma^2 \times 10^3$ (Å^2)		$C_3 \times 10^4$ (Å^3)	
bonds	*f*	*a*	*f*	*a*	*f*	*a*	*f*	*a*
Zn−O	3.9	4.9	1.98	2.00	8.9	9.8	0	10.9
Zn−O		1.2		2.79		3.2		
Zn−Sn	1.0	1.2	3.18	3.75	11.0	6.7	30	
Zn−Zn		3.9		3.82		11.6		

[a] S_0^2 = 0.90, ΔE ∼ 4.9 eV, k = 2.4−10.5 Å^{-1}, and R = 1.0−4.0 Å. Figure of merit *R*-factor <0.01. See Figure S5 for the fits.

Aging Effect on Surface Sn Sites. In contrast to Zn, hydration around the Sn sites is much less obvious. In a structural study of Sn(II) in hyper-alkaline aqueous solution, Bajnóczi et al. showed that the Sn K edge XANES of the

DOI: 10.1021/acs.jpcc.8b09412
J. Phys. Chem. C 2018, 122, 28151−28157

$[Sn(OH)_3]^-$ complex has a prominent shoulder at ~16 eV after the whiteline and that only the Sn−O bonds are observed by EXAFS at ~2.08 Å.[19] The effect of the H 1s state on the Sn−O bonding orbital is thus likely similar to that on the Zn−O bond. Figure 5 compares the Sn K edge XANES measured

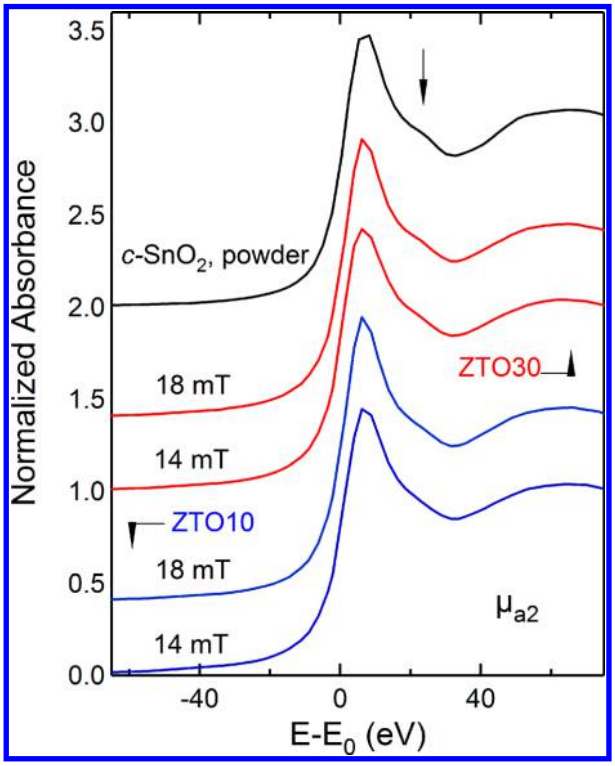

Figure 5. Comparison of surface Sn K edge XANES. Crystalline SnO_2 is also shown.

on aged film surfaces; powder *c*-SnO_2 is also shown. A shoulder is seen around ~20 eV (arrow). It is more prominent on the *a*-ZTO30−18 mT film surface for which strong hydration on the surface Zn sites has occurred. The shoulder for *c*-SnO_2 is due to the EXAFS oscillation of the dihedral Sn−O interaction centered at 4.0 Å. The interaction at this length does not appear in the Sn K edge EXAFS of the *a*-ZTO films (see, e.g. Figure S5) or the *a*-SnO_2 film.[20] Therefore, the more prominent shoulder found on the *a*-ZTO30−18 mT film surface may be associated with hydration of the surface. Interestingly, the surface XANES (not shown) of the *a*-SnO_2 film whose ρ is the lowest (Figure 2B) shows no clear shoulder. Therefore, the low density argument may not be a prerequisite for hydration to occur as far as the Sn site is concerned. Compared to the Zn site, the Sn site is much less stressed. It is speculated that a physical and/or chemical interplay may play a role in the relationship between the Sn sites and hydrated Zn sites, the latter of which are abundant on the *a*-ZTO30−18 mT film surface.

Structural Change at Surface Sn Sites. The Sn−K edge EXAFS results are presented in Table 2 for the films whose structures around Zn show appreciable changes. The result on *a*-SnO_2 is also presented for comparison. Square brackets indicate the results that are obtained when the root-mean-square σ is set to that of as-deposited ZTO30−18 mT to have an appreciation of the correlation between N and σ. As is shown, the structure around Sn is essentially the same for as-deposited films. The small N (<6) on the surface may be an

Table 2. Surface Structures around Sn of As-Deposited (*f*) and Aged (*a*) Films[a]

samples		N	R (Å)	σ^2 (Å^2)	C_3 (Å^3)
ZTO30	18 mT (*f*)	5.3	2.09	0.0066	4.8×10^{-4}
	18 mT (*a*)	4.9	2.11	0.0057	11.6×10^{-4}
		[5.2]	[2.12]	[0.0066]	[12.2×10^{-4}]
ZTO10	18 mT (*f*)	5.3	2.07	0.0066	4.9×10^{-4}
	18 mT (*a*)	5.7	2.06	0.0065	
SnO_2	22 mT (*f*)	5.3	2.08	0.0063	4.5×10^{-4}
	22 mT (*a*)	5.8	2.08	0.0079	4.0×10^{-4}

[a]The scaling factor $S_0^2 = 1.02$. Energy shift $\Delta E = 6.0 \pm 1.0$ eV. Error bars for N are within ±0.3 and for R within ±0.01 Å. [ ] includes the results obtained by setting σ^2 to that of as-deposited ZTO30−18 mT. The R-factor ranges from 0.0016−0.0037.

analogue to surface reconstruction on the *c*-SnO_2 (110) surface where five coordinate Sn, bridging O, and O vacancy coexist.[21] Upon aging, N is smaller or remains the same for the ZTO30 films but is larger for the ZTO10 films. The latter is corroborated by a clear increase in the whiteline intensity (Figure S6). The structure of the Sn-rich films (ZTO10) is consistent with the *a*-SnO_2 structure. Therefore, surface Sn sites relax differently depending on film composition. For the ZTO10 films, the increased Sn−O coordination suggests a decrease of the number of dangling bonds or vacancies.

It is worth pointing out that the elevated absorption before the rise of the Sn K edge for the surface over film bulk (Figure 1B and also see Figure S6c) may result from the presence of negatively charged dangling bonds[22] on Sn or from 5-fold coordinated Sn surface termination.[21] Such an electronic configuration (reducing in nature, or equivalently noted as V_O' in the Kröger−Vink notation) screens the corehole on Sn, effectively lowering the energies of available empty states. Similar observations are attributed to vacancies in various systems.[23,24] This is not seen for the Zn K edge XANES (Figure 1B) because the surface Zn is fully coordinated (Table 1).

4. DISCUSSION

As described above, the surfaces of *a*-ZTO films undergo structural changes over time, the extent of which is governed by film composition and density. The changes are incurred by dissociative H_2O/O_2 adsorption on the surfaces. Figure 6 illustrates the surface structure and our understanding of the surface stability. Water and O_2 dissociation on *c*-ZnO or *c*-SnO_2 are catalyzed by steps or "discontinuities" associated with various sites and defects.[25,26,21] Similar mechanisms can operate on the *a*-ZTO film surfaces. The low density films have an open structure that may be prone to physisorption, and the film surface energy may be higher near the Zn sites, which could facilitate a dissociative reaction. Clearly, low density is not the only determinant, since the *a*-SnO_2 film has the lowest density but shows little hydration. The surface Zn sites appear to be effective in H_2O dissociation when the density is low. The local strain around these Zn sites (Zn sits in a Sn site with $N \sim 4$) may play a crucial role in catalyzing the reaction.[27] However, the *a*-ZTO30−14 mT film shows a weak hydration, albeit a relative low density (Figures 2B and 3B).

Numerous studies have shown that the *c*-SnO_2 surfaces are active in H_2O dissociation.[28,29] Therefore, the weak hydration on the *a*-SnO_2 surface and at the surface Sn sites of the *a*-ZTO films is somewhat surprising. The prominent shoulder for the

DOI: 10.1021/acs.jpcc.8b09412
J. Phys. Chem. C 2018, 122, 28151−28157

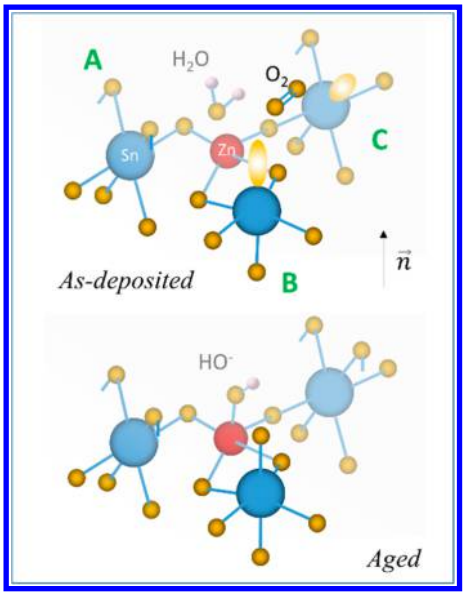

Figure 6. A model illustration of surface structure based on the results presented in the main text. $\vec{n}$ represents the surface normal direction. Upper: surface of as-deposited film. Lower: surface of aged film. Sn, blue; Zn, dark red; O, yellow; and H, purple. The orientation of the Zn site satisfies the X-ray polarization dependent GIXAS measurements. (A) Bridging O termination. (B) Five-coordinate Sn termination. (C) Bridging O vacancy. O_2 dissociation involving both vacant sites,[21] i.e., on the Sn termination (B) and on the bridging-O termination (C).

a-ZTO30−18 mT film (Figure 5) may not be attributable to direct OH− attachments to the Sn sites because it is not supported by the structural results presented in Table 2 (no changes in N over time). It is speculated here that apart from OH^- attachments, such a shoulder could also result from interaction between polar water molecules and dangling bonds on Sn and/or between the OH^- ligand on Zn and the dangling bonds, a "proximity effect", say, through van der Waals interaction. The latter is more likely on the *a*-ZTO30−18 mT surface on which the hydrated Zn sites are abundant.

For the *a*-ZTO10 films and the *a*-SnO_2 film, the increase in *N* around Sn was unambiguously measured (Table 2). The source of oxygen may be from water dissociation on the Zn sites and/or O_2 dissociation. The Sn-rich surfaces may be more prone to the exothermal O_2 dissociation in the way observed on the *c*-SnO_2 (110) surface, on which $[SnO_5]$:$[SnO_6]$ = 1:1,[21] i.e., the average coordination number of 5.5. The *a*-SnO_2 surface and the Sn-occupied area on the *a*-ZTO surfaces may imitate such a reconstruction (for which $N \sim 5.5$). This reaction requires participation of both $[SnO_5]$ sites and bridging-O vacancies.[21] As a result, one oxygen is added onto $[SnO_5]$, and the second one occupies the bridging vacancy, resulting the increase in *N* around Sn. We argue that the Sn sites on the *a*-ZTO30 film surfaces may be less reactive through this channel because they are strongly influenced by the adjacent Zn sites. As a result, *N* around Sn remains unchanged on these surfaces over time (Table 2).

5. CONCLUSIONS

The structure and chemistry of *a*-ZTO film surfaces and their evolution over time are characterized and accounted for in the atomistic details. The interplay between the surface chemistry and structure was illustrated and conforms to the knowledge and principles established for crystalline systems. We show that the surface chemistry of these amorphous films can vary markedly with film composition and density. The surfaces of low density *a*-ZTO films are vulnerable and react to ambient atmosphere, in particular if the composition is too far off the solubility limit.[13] Although the compositional flexibility of amorphous films is advantageous, caution needs to be taken, e.g., regarding to their long-term stability. It is unknown what impact the changes in surface chemistry has on even longer-term stability of the films. So far, there have no detrimental effects on their electrical properties. The electrical conductivities (not shown) of both *a*-ZTO30−18 mT and *a*-ZTO10−18 mT films, in fact, increased by ∼10% over this time as t^n; $n \sim 0.5$ and 0.56. These increases may be related to structural relaxation within the films induced by the surface changes presented here. This will be the focus of our future work.

■ ASSOCIATED CONTENT

Supporting Information

The Supporting Information is available free of charge on the ACS Publications website at DOI: 10.1021/acs.jpcc.8b09412.

S1: Setup for surface X-ray absorption and reflectivity measurements; S2: Extended X-ray absorption fine structure; S3: XRR and XPS characterizations; S4: Comparison of surface XANES; S5: Quantitative analyses of the EXAFS data (PDF)

■ AUTHOR INFORMATION

Corresponding Author

*E-mail: q-ma@northwestern.edu.

ORCID

Tobin J. Marks: 0000-0001-8771-0141
Michael J. Bedzyk: 0000-0002-1026-4558
Qing Ma: 0000-0001-6530-9322

Notes

The authors declare no competing financial interest.

■ ACKNOWLEDGMENTS

This work was performed at the DuPont-Northwestern-Dow Collaborative Access Team (DND-CAT) located at Sector 5 of the Advanced Photon Source (APS). DND-CAT is supported by Northwestern University (NU), E.I. DuPont de Nemours & Co., and The Dow Chemical Company. This research used resources of the APS, a U.S. Department of Energy (DOE) Office of Science User Facility operated for the DOE Office of Science by Argonne National Laboratory under Contract DE-AC02-06CH11357. Part of this work was supported by the National Science Foundation (NSF) MRSEC Program DMR 1121262 at the Materials Research Center of NU. This work made use of the J. B. Cohen X-ray Diffraction Facility and the MatCI Facilities at NU, supported by the MRSEC program of NSF and NU. Ellipsometry was performed in the Keck-II facility of the NUANCE Center at NU. NSF-NSEC, NSF-MRSEC, Keck Foundation, the State of Illinois, and NU support the NUANCE Center. S.L.M. acknowledges support of an NSF Graduate Research Fellowship.

DOI: 10.1021/acs.jpcc.8b09412
J. Phys. Chem. C 2018, 122, 28151−28157

REFERENCES

(1) Kamiya, T.; Nomura, K.; Hosono, H. Present Status of Amorphous In−Ga−Zn−O Thin-Film Transistors. *Sci. Technol. Adv. Mater.* **2010**, *11*, 044305.

(2) Buchholz, D. B.; Ma, Q.; Alducin, D.; Ponce, A.; Jose-Yacaman, M.; Khanal, R.; Medvedeva, J. E.; Chang, R. P. H. The Structure and Properties of Amorphous Indium Oxide. *Chem. Mater.* **2014**, *26*, 5401−5411.

(3) Zhu, Q.; Ma, Q.; Buchholz, D. B.; Chang, R. P. H.; Bedzyk, M. J.; Mason, T. O. Structural and Physical Properties of Transparent Conducting, Amorphous Zn-doped SnO_2 Films. *J. Appl. Phys.* **2014**, *115*, 033512.

(4) Moffitt, S. L.; Zhu, Q.; Ma, Q.; Falduto, A.; Buchholz, D. B.; Chang, R. P. H.; Mason, T. O.; Medvedeva, J. E.; Marks, T. J.; Bedzyk, M. J. Probing the Unique Role of Gallium in Amorphous Oxide Semiconductors Through Structure − Property Relationships. *Adv. Electron. Mater.* **2017**, *3* (10), 1700189.

(5) Cui, B.; Zeng, L.; Keane, D.; Bedzyk, M. J.; Buchholz, D. B.; Chang, R. P. H.; Yu, X.; Smith, J.; Marks, T. J.; Xia, Y.; Facchetti, A. F.; Medvedeva, J. E.; Grayson, M. Thermal Conductivity Comparison of Indium Gallium Zinc Oxide Thin Films: Dependence on Temperature, Crystallinity, and Porosity. *J. Phys. Chem. C* **2016**, *120*, 7467−7475.

(6) Liu, J.; Buchholz, D. B.; Chang, R. P.; Facchetti, A.; Marks, T. J. High-Performance Flexible Transparent Thin-Film Transistors Using a Hybrid Gate Dielectric and an Amorphous Zinc Indium Tin Oxide Channel. *Adv. Mater.* **2010**, *22* (21), 2333−2337.

(7) Minami, T.; Takata, S.; Sato, H.; Sonohara, H. Properties of Transparent Zinc-Stannate Conducting Films Prepared by Radio Frequency Magnetron Sputtering. *J. Vac. Sci. Technol., A* **1995**, *13* (3), 1095−1099.

(8) Kim, H.-M.; Jung, S.-K.; Ahn, J.-S.; Kang, Y.-J.; Je, K.-C. Electrical and Optical Properties of In_2O_3−ZnO Films Deposited on Polyethylene Terephthalate Substrates by Radio Frequency Magnetron Sputtering. *Jpn. J. Appl. Phys., Part 1* **2003**, *42* (1), 223−227.

(9) Hara, H.; Hanada, T.; Shiro, T.; Yatabe, T. Properties of Indium Zinc Oxide Thin Films on Heat Withstanding Plastic Substrate. *J. Vac. Sci. Technol., A* **2004**, *22* (4), 1726−1729.

(10) Zhu, Q. Physical Properties and Local Structures of Amorphous Zn-Sn−O and Amorphous In-Ga-O Films. Ph.D. Thesis, Northwestern University: Evanston, 2013.

(11) Moffitt, S. L.; Adler, A. U.; Gennett, T.; Ginley, D. S.; Perkins, J. D.; Mason, T. O. Confirmation of the Dominant Defect Mechanism in Amorphous In-Zn-O Through the Application of In Situ Brouwer Analysis. *J. Am. Ceram. Soc.* **2015**, *98* (7), 2099−2103.

(12) Chattopadhyay, D. Endangered Elements of the Periodic Table. *Resonance* **2017**, *3* (11), 75−81.

(13) Gouvea, D.; do Rosario, D. C. C.; Caliman, L. B. Surface and Grain-Boundary Excess of ZnO-Doped SnO_2 Nanopowders by the Selective Lixiviation Method. *J. Am. Ceram. Soc.* **2017**, *100*, 4331−4340.

(14) Becker, R. S.; Golovchenko, J. A.; Patel, J. R. X-Ray Evanescent-Wave Absorption and Emission. *Phys. Rev. Lett.* **1983**, *50* (3), 153−156.

(15) Martens, G.; Rabe, P. EXAFS Studies on Superficial Regions by Means of Total Reflection. *Phys. Stat. Sol. (a)* **1980**, *58*, 415−424.

(16) Moffitt, S. L.; Ma, Q.; Buchholz, D. B.; Chang, R. P. H.; Bedzyk, M. J.; Mason, T. O. Grazing Incidence X-Ray Absorption Characterization of Amorphous Zn-Sn−O Thin Film. *J. Phys.: Conf. Ser.* **2016**, *712*, 012116.

(17) Parratt, L. G. Surface Studies of Solids by Total Reflection of X-Rays. *Phys. Rev.* **1954**, *95* (2), 359−369.

(18) Bunau, O.; Joly, Y. Self-Consistent Aspects of X-Ray Absorption Calculations. *J. Phys.: Condens. Matter* **2009**, *21*, 345501.

(19) Bajnóczi, E. G.; Czeglédi, E.; Kuzmann, E.; Homonnay, Z.; Bálint, G.; Sipos, P.; Persson, I. Speciation and Structure of Tin(II) in Hyper-Alkaline Aqueous Solution. *Dalton Trans.* **2014**, *43*, 17971.

(20) Zhu, Q.; Ma, Q.; Buchholz, D. B.; Chang, R. P. H.; Bedzyk, M. J.; Mason, T. O. Structural Anisotropy in Amorphous SnO_2 Film Probed by X-Ray Absorption Spectroscopy. *Appl. Phys. Lett.* **2013**, *103*, 031913.

(21) Slater, B.; Catlow, C. R. A.; Williams, D. E.; Stoneham, A. M. Dissociation of O_2 on the Reduced SnO_2 (110) Surface. *Chem. Commun.* **2000**, 1235−1236.

(22) Lannoo, M. The Role of Dangling Bonds in the Properties of Surfaces and Interfaces of Semiconductors. *Rev. Phys. Appl.* **1990**, *25*, 887−894.

(23) Ma, Q.; Prater, J. T.; Sudakar, C.; Rosenberg, R. A.; Narayan, J. Defects in Room-Temperature Ferromagnetic Cu-doped ZnO Films Probed by X-Ray Absorption Spectroscopy. *J. Phys.: Condens. Matter* **2012**, *24*, 306002.

(24) Huber, S. P.; Gullikson, E.; Meyer-Ilse, J.; Frye, C. D.; Edgar, J. H.; van de Kruijs, R. W. E.; Bijkerk, F.; Prendergast, D. Detection of Defect Populations in Superhard Semiconductor Boron Subphosphide B12P2 Through X-Ray Absorption Spectroscopy. *J. Mater. Chem. A* **2017**, *5* (12), 5737−5749.

(25) Önsten, A.; Stoltz, D.; Palmgren, P.; Yu, S.; Göthelid, M.; Karlsson, U. O. Water Adsorption on ZnO(0001): Transition from Triangular Surface Structures to a Disordered Hydroxyl Terminated Phase. *J. Phys. Chem. C* **2010**, *114*, 11157−11161.

(26) Hu, H.; Ji, H.-F.; Sun, Y. The Effect of Oxygen Vacancies on Water Wettability of a ZnO Surface. *Phys. Chem. Chem. Phys.* **2013**, *15*, 16557−16565.

(27) Song, Z.; Fan, J.; Xu, H. Strain-Induced Water Dissociation on Supported Ultrathin Oxide Films. *Sci. Rep.* **2016**, *6*, 22853.

(28) Vlček, L.; Cummings, P. T. Adsorption of Water on TiO_2 and SnO_2 Surfaces. *Collect. Czech. Chem. Commun.* **2008**, *73* (4), 575−589.

(29) Kumar, N.; Kent, P. R. C.; Bandura, A. V.; Kubicki, J. D.; Wesolowski, D. J.; Cole, D. R.; Sofo, J. O. Faster Proton Transfer Dynamics of Water on SnO_2 Compared to TiO_2. *J. Chem. Phys.* **2011**, *134*, 044706.

DOI: 10.1021/acs.jpcc.8b09412
J. Phys. Chem. C 2018, 122, 28151−28157